V.M. Gun'ko, O.I. Oranska, V.V. Paientko, I.Ya. Sulym

PARTICULATE MORPHOLOGY OF NANOSTRUCTURED MATERIALS

Chuiko Institute of Surface Chemistry of National Academy of Sciences of Ukraine
17 General Naumov Str., Kyiv, 03164, Ukraine, E-mail: vlad_gunko@ukr.net

The aim of this study was to develop a technique to analyze the crystalline and particulate morphology of highly disperse complex metal and metalloid oxides, which include both crystalline and amorphous phases, using X-ray diffraction (XRD) data to compute crystallite size distributions (CSD) compared to the particles size distribution functions estimated from high-resolution transmission electron microscopy (TEM) images treated with specific software. Two versions of the XRD treatment methods were used: (i) full profile analysis (FPA) of whole XRD patterns with a self-consistent regularization (SCR) procedure using models for spherical and lamellar crystallites that allows us to estimate relative contributions of crystallites of different shapes; and (ii) analysis of main pure XRD lines with consideration of corrections on an instrumental line profile and background using a regularization procedure with models of spherical or lamellar crystallites. The XRD and TEM based approaches were tested to analyze the crystalline and particulate morphology of various disperse materials: complex (binary and ternary) fumed oxides with silica/alumina, silica/titania, and alumina/silica/titania including crystalline alumina and titania and amorphous silica; nanocomposites $CeO_2–ZrO_2/SiO_2$ (10 : 10 : 80 wt.%) and $TiO_2–ZrO_2/SiO_2$ (10 : 10 : 80 wt.%) including crystalline and amorphous phases and synthesized using a liquid-phase method and fumed silica A–300 as a substrate; and natural clays of complex composition including several crystalline phases. Obtained results show that the developed approaches to analyze the XRD patterns could be effectively used to compute the CSD in parallel with TEM image treatments, using specific software, for a deeper insight into crystalline and particulate morphology of various disperse materials.

Keywords: *complex fumed oxides, deposited oxides, clays, particulate morphology, crystallite size distribution*

INTRODUCTION

The particulate morphology (PM) plays an important role on applications of disperse materials such as adsorbents, fillers, catalysts, thickeners, carriers, *etc.* [1–5]. There are such direct methods to analyze the PM as transmission (TEM) and scanning (SEM) electron microscopies and atom force microscopy [6, 7]. Accurate treatment of the corresponding images with specific software gives the particle size distribution (PaSD) functions. Additionally, there are various methods giving indirect information on the PM such as small angle X-ray (or neutron) scattering (SAXS) [8–10], X-ray diffraction (XRD) [11–13], dynamic and static light scattering [14, 15], adsorption (for nonporous nanoparticles of fumed oxides) [16, 17] and other methods. Some of these methods give information on amorphous and crystalline particles, but others describe only crystalline phases. In the case of complex particles including several crystalline and amorphous phases, to obtain more accurate information, several methods from two mentioned groups (direct vs.

indirect ones) should be used. The XRD data could be used for simple estimation of average sizes of crystallites (d_{cr}) using Scherrer or Debye–Scherrer equations [12, 18]. Additionally, the XRD data could be used to estimate the crystallite size distribution (CSD) functions using full profile analysis of selected lines or total XRD patterns [19, 20]. To calculate the broadened line (pure) profile related to the crystallite size/faulting effects of materials studied, as well a size distribution function, one could use two integral equations[19, 20]:

$$I_{ex.obs.}(\varepsilon) = C \int h_{i.p.}(\varepsilon - t) i_{ex.pure}(t) dt \,, \qquad (1)$$

$$i(s) = \int_{D_{min}}^{D_{max}} D \frac{\sin^2(\pi s D)}{(\pi s D)^2} g(D) dD \,, \qquad (2)$$

where $I_{ex.obs.}(\varepsilon)$ is the experimentally observed X-ray diffraction profile, C is a constant, $h_{i.p.}$ is the instrumental profile, $i(s)$ is the pure crystallite size/faulting profile, D is the crystallite size, $g(D)$ is the CSD function, 2θ is the scattering angle, $2\theta_{hkl}$ is the scattering angle corresponding to a peak [19]

$$s = s_{2\theta} - r_{hkl} = \frac{2\sin\theta}{\lambda} - \frac{2\sin\theta_{hkl}}{\lambda}.$$

The variable ε in eq. (1) corresponds to the angular deviation of a point from the true Bragg angle $2\theta_0$; and ε and the auxiliary variable t have the dimension of 2θ.

The CSD function $g(D)$ could be computed by solving integral eq. (1) and then eq. (2) (note that eq. (2) corresponds to spherical crystallites) with a regularization procedure, *e.g.* CONTIN [21]. This approach could be applied to a selected line or to the full profile of total XRD patterns analyzed after background subtraction and normalization. The aim of this study is to analyze the XRD data for various metal or metalloid oxides (MO) such as fumed MO (FMO) (Figs. 1–4, Table), oxides deposited onto fumed silica (Figs. 5 and 6), and natural clays (Figs. 7–9), to obtain the CSD functions compared to the PaSD functions computed using TEM images treated with ImageJ (granulometry plugin) [22].

MATERIALS

Several individual, binary, and ternary FMO (Table) including crystalline phases of titania (both anatase and rutile) and alumina (several phases) and completely amorphous silica (Pilot plant of Chuiko Institute of Surface Chemistry, Kalush, Ukraine) were used here and described in detail elsewhere [23–25]. Nanocomposites $CeO_2–ZrO_2/SiO_2$ (10 : 10 : 80 wt. %) and $TiO_2–ZrO_2/SiO_2$ (10 : 10 : 80 wt. %) were synthesized using a liquid-phase method and fumed silica A-300 as a substrate that results in the formation of $ZrCeO_x/SiO_2$ and $ZrTiO_x/SiO_2$ heated at 550 °C (XRD-amorphous phase, but HRTEM images show the presence of crystallites) and 1100 °C (including XRD-crystalline phase) [26–28]. Two natural materials: "black clay" (Carpathian region including crystalline α–quartz, $CaCO_3$, smectite with amorphous carbon (coal) and other components) and kaolin clay (Azov region, mainly kaolinite and small admixtures with α–quartz and clays, *e.g.* muscovite/illite) were studied here (see some details on these clays in [29]).

X-RAY POWDER ANALYSIS

X-ray diffraction patterns for some samples were recorded at room temperature using a DRON-3M diffractometer (Burevestnik, St.-Petersburg, Russia) with CuK_α ($\lambda = 0.15418$ nm) radiation and a Ni filter in the 2θ range from 10 to 70°.

XRD patterns of FMO and clay samples were recorded over $2\theta = 4–80°$ range using a DRON–4–07 (Burevestnik, St. Petersburg) diffractometer with CuK_α radiation and a Ni filter. Analysis of the crystalline structures was carried out using the JCPDS Database (International Center for Diffraction Data, PA, 2001) [30]. To estimate the instrumental line profile ($h_{i.p.}$ in eq. (1)), XRD pattern of large crystallites (> 100 nm) of silicon was used.

HIGH-RESOLUTION TRANSMISSION ELECTRON MICROSCOPY (HRTEM)

The particulate morphology of $CeO_2–ZrO_2/SiO_2$ and $TiO_2–ZrO_2/SiO_2$ samples preheated at 550 °C was analyzed using Transmission Electron Microscope (TEM) employing a Tecnai G2 T20 X-TWIN (FEI Co., USA) apparatus operating at voltage of 200 kV with LaB_6 electron source. The presence of metals and their elemental composition were recorded by using energy dispersive X-ray (EDX). The samples were supported on holey carbon copper grids by dropping ethanol suspensions containing uniformly dispersed oxide powders.

HRTEM (JEM–2100F, Japan) images of FMO were recorded for powder samples added to acetone (for chromatography) and sonicated. Then a drop of the suspension was deposited onto a copper grid with a thin carbon film. After acetone evaporation, sample particles remained on the film were studied with HRTEM.

RESULTS AND DISCUSSION

Complex binary (SA, ST) and ternary (AST) fumed oxides (Table) include crystalline alumina and titania, but silica is always amorphous (Fig. 1) [23, 24, 31]. For ST samples, titania (both anatase and rutile phases) crystallites are typically embedded into silica shells (Fig. 2 *b*, *c*). For SA (Fig. 2 *a*), both large polycrystalline and small particles (crystallites) are observed as well for AST [31]. During pyrogenic synthesis, $AlCl_3$ used as a precursor should be sublimated, and its reactivity differs from that of $SiCl_4$ and $TiCl_4$ that results in enhanced nonuniformity of complex binary and ternary FMO (Fig. 2) [24, 31]. In the case of fumed ST20 and TiO_2 (20 wt. %)

deposited onto A–300 as well AST1, amorphous silica significantly contributes the XRD patterns (Fig. 1). For other FMO samples, contribution of amorphous phases is much smaller that allows us to use eqs. (1) and (2) to compute the CSD functions with a regularization procedure for total XRD patterns. In the case of full profile analysis (FPA) of the total XRD patterns, the regularization procedure was modified to self-consistent regularization (SCR) previously used to treat nitrogen adsorption (models of slitshaped and cylindrical pores and voids between spherical nanoparticles) and SAXS (models of spherical, cylindrical and lamellar particles) data [16, 17, 31, 32]. An additional advantage of the SCR procedure is the possibility to estimate weight contributions of pores or particles (or crystallites) of different shapes.

The FPA applied with the SCR procedure (using spherical and lamellar models of crystallites) without corrections on the instrumental line profile due to equipment effects provides appropriate fitting of total XRD pattern

(Fig. 3 *a*). However, in this approach, the CSD could give smaller sizes of crystallites than those observed in HRTEM images since the broader the line, the smaller is the corresponding crystallite. Therefore, the CSD functions (Fig. 4) were also computed using the main lines of crystalline titania: anatase ($2\theta \approx 25.3°$) and rutile (27.4°), and crystalline alumina (67.1°) with consideration of the instrumental line profile due to equipment effects. An increase in titania amounts in ST and AST results in an increase in sizes of titania crystallites (Fig. 4) (the corresponding XRD lines become narrower) because growing of titania particles (cores in core-shell particles) is faster in the flame than silica particles (shells). In the case of fumed ST20 and titania (20 wt. %) deposited onto A-300, the CSD functions are similar due to the same amounts of titania and the same second (silica) phase. Minimal sizes of crystallites are observed for alumina alone or SA and AST samples (Fig. 4) that is in agreement with TEM images (Fig. 2 *d, f*).
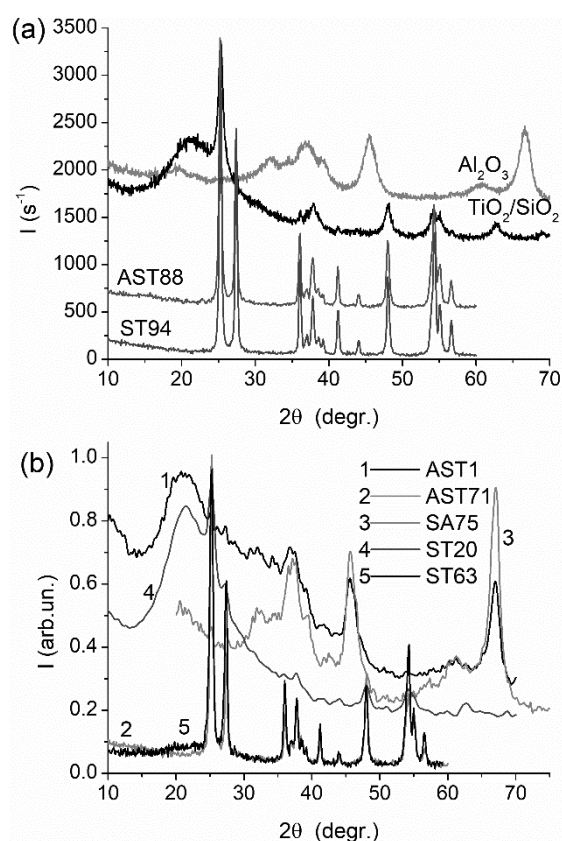

Fig. 1. XRD patterns for fumed oxides: (*a*) mixed δ,γ,θ-alumina, silica/titania ST94 (94 wt. % TiO$_2$), alumina/silica titania AST88 (88 wt. % TiO$_2$), and titania (20 wt. % TiO$_2$) deposited onto fumed silica; (*b*) FMO with alumina/silica/titania with 1 (AST1) and 71 (AST71) wt. % TiO$_2$, silica/alumina at 75 wt. % Al$_2$O$_3$, and silica/titania with 20 (ST20) and 63 (ST63) wt. % TiO$_2$
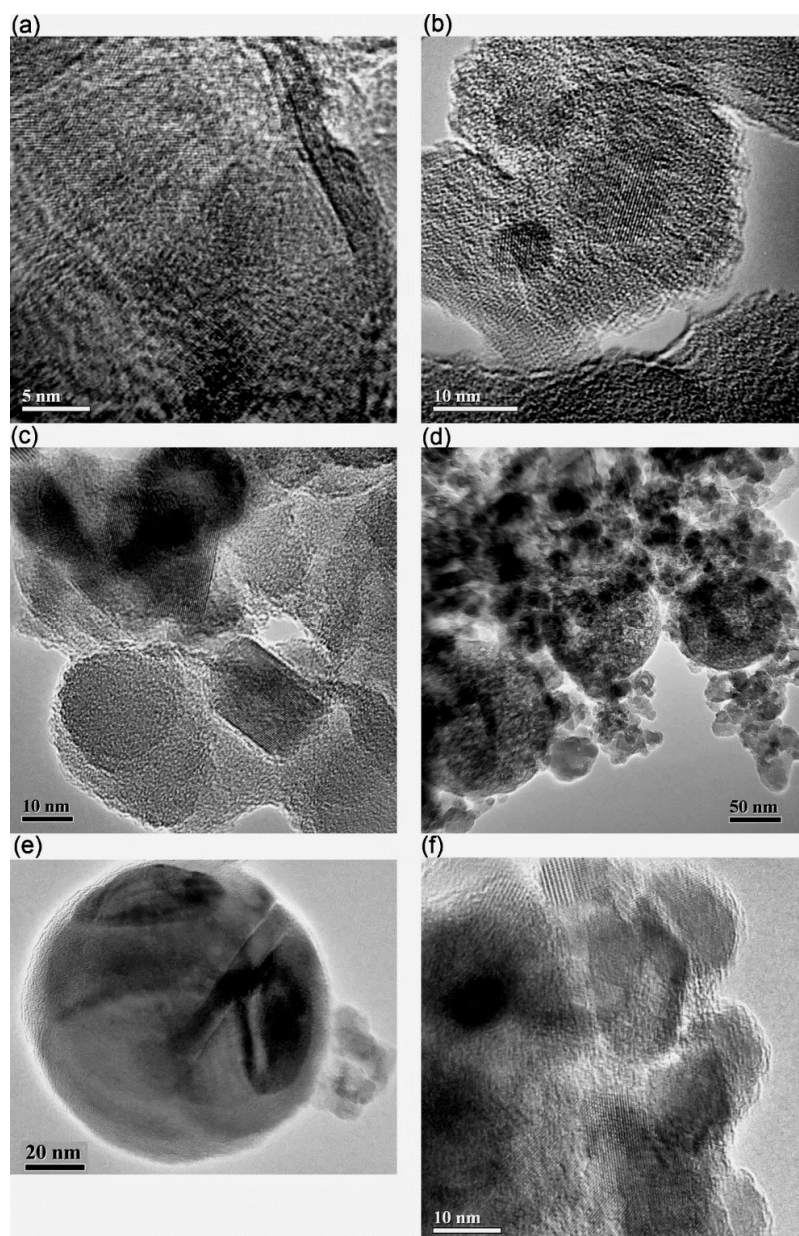
Fig. 2. HRTEM images of FMO: (*a*) SA75, (*b*) ST20, (*c*) ST63, (*d*) AST1, (*e*) AST50, (*f*) AST71

Table. Composition, specific surface area (S_{BET}) and pore volume (V_p) of fumed oxides

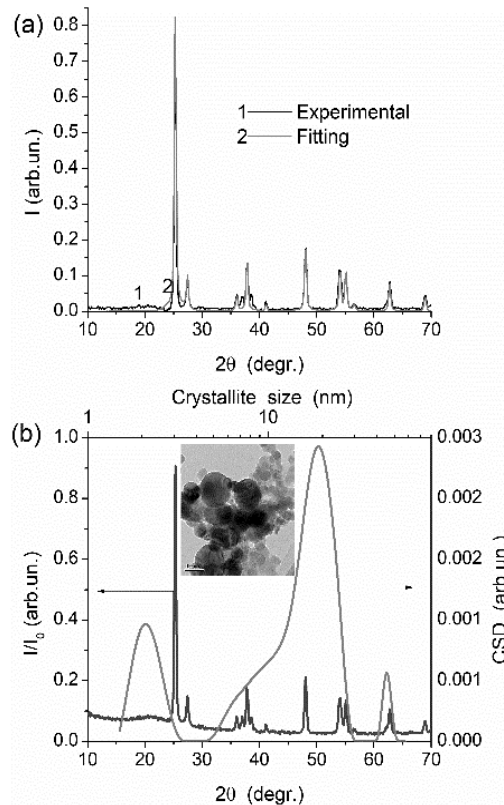| Sample	C_{SiO_2} (wt. %)	C_{TiO_2} (wt. %)	$C_{Al_2O_3}$ (wt. %)	S_{BET} (m^2/g)	V_p (cm^3/g)
A-300	99.8	–	–	294	0.524
Al$_2$O$_3$			100	125	0.262
SA75	25	–	75	118	0.320
ST20	80	20	–	84	0.174
ST63	33	63	–	84	0.215
ST94	6	94	–	30	0.100
AST1	10	1	89	99	0.253
AST50	28	50	22	37	0.095
AST71	8	71	21	74	0.127
AST88	8	88	4	39	0.123

Fig. 3. (*a*) Normalized XRD pattern and FPA fitting for AST50, (*b*) XRD pattern and CSD for AST50
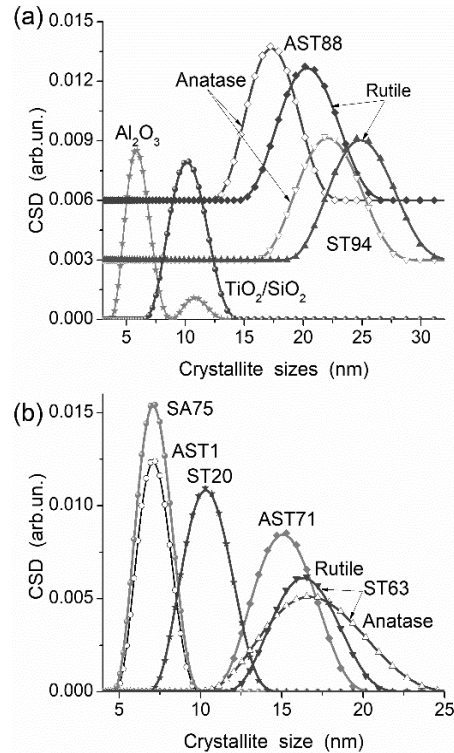

Fig. 4. CSD for fumed oxides, calculated for main peaks using pure line profile with corrections on the equipment effects, at C_{TiO2} of (*a*) 20 (deposited onto A-300), 88 and 94 wt.% and (*b*) 1, 20, 63 and 71 wt.% (contributions of anatase and rutile are shown for AST88, ST94, and ST63) and crystalline alumina in some samples
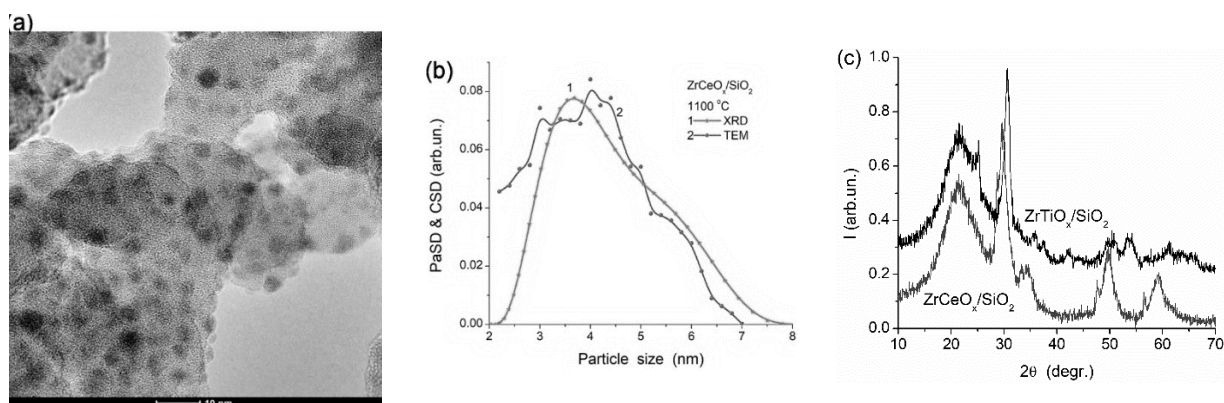
Fig. 5. (*a*) TEM image (preheating at 550 °C), (*b*) CSD based on XRD (preheating at 1100 °C) (main peak of ZrCeO$_x$ with correction) and TEM image for ZrCeO$_x$/SiO$_2$, (*c*) normalized XRD patterns of ZrCeO$_x$/SiO$_2$ and ZrTiO$_x$/SiO$_2$ (preheated at 1100 °C)

Direct comparison of the CSD (XRD) and PaSD (HRTEM) (Figs. 5 and 6) shows that the latter can include both crystalline and amorphous phases. This is well seen for ZrTiO$_x$/SiO$_2$ sample (Fig. 6). As a whole, the sizes of crystallites estimated using corrected (pure) XRD lines correspond to the crystallite sizes (preheating at 1100°C) observed in HRTEM images (preheating at 550 °C, crystallites are observed in TEM images, but XRD does not sense them in contrast to samples preheated at 1100 ºC [26-28]) with maximal magnification for ZrTiO$_x$/SiO$_2$ and ZrCeO$_x$/SiO$_2$ (Figs. 5 and 6).

More complex XRD patterns are observed for natural oxides, *e.g.* clays (Fig. 7) due to presence

of several oxide phases of various shapes including nearly spherical (quartz) and larger lamellar (kaolinite and other clays) structures (Fig. 8) [29]. Therefore, the SCR/FPA procedure was used with two models for spherical and lamellar crystallites. Note that the SCR procedure gives a strongly major contribution of lamellar crystallites for clays studied. In the case of corrected XRD data on the instrumental line profile, the analysis was carried out for the main lines in the XRD patterns. The SCR/FPA without any experimental correction gives smaller crystallite sizes similar to those observed for other materials studied (Fig. 9).
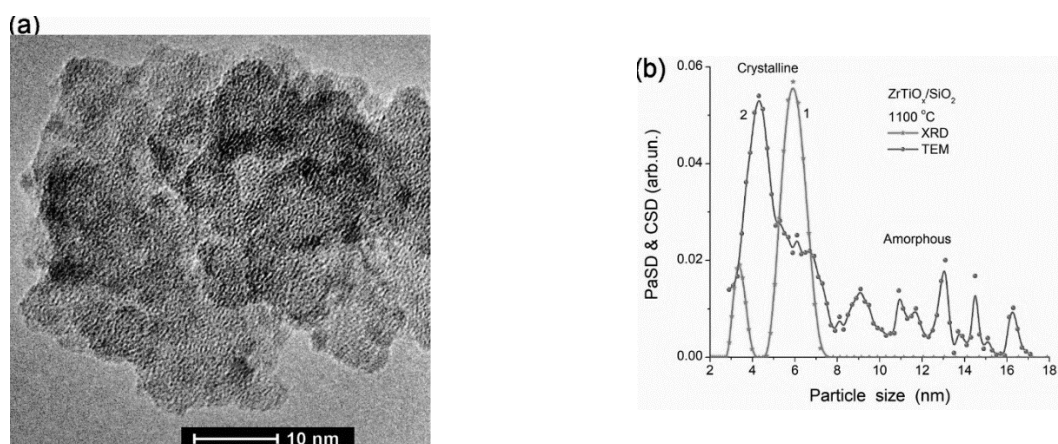

Fig. 6. (*a*) HRTEM image (preheating at 550 °C) and (*b*) CSD based on XRD (preheating at 1100 °C) pattern (main peak of ZrTiO$_x$ with correction) and TEM image for ZrTiO$_x$/SiO$_2$
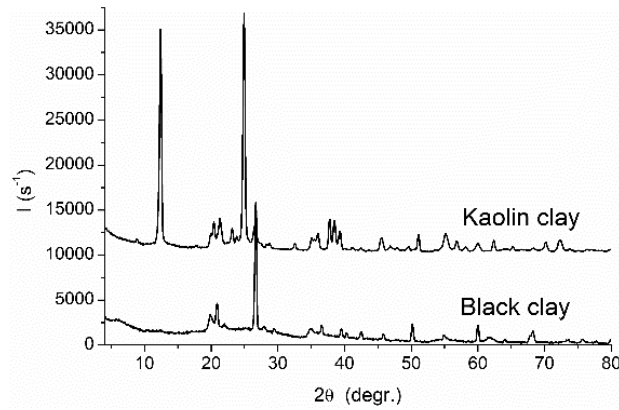
Fig. 7. XRD patterns for kaolin clay (two main peaks at 12.4° (001) and 25° (002) correspond to kaolinite at average crystallite sizes d_{cr} = 18 nm (hkl – 111) and 28 nm (hkl – 002) (estimated with Scherrer eq.), there are some other clays, such as muscovite/illite/halloysite and α–quartz as admixtures) and black clay (main peak (101) at 26.7° corresponds to α-quartz at $d_{cr} \approx 52$ nm, 20.8° – α–quartz, 19.8° – smectite, and some other clays (kaolinite, muscovite) as admixtures, as well an amorphous part, *e.g.*, a certain halo at 15°< 2θ < 35° and an increase in intensity at 2θ < 15°, related to coal and other components) (see details in [29])
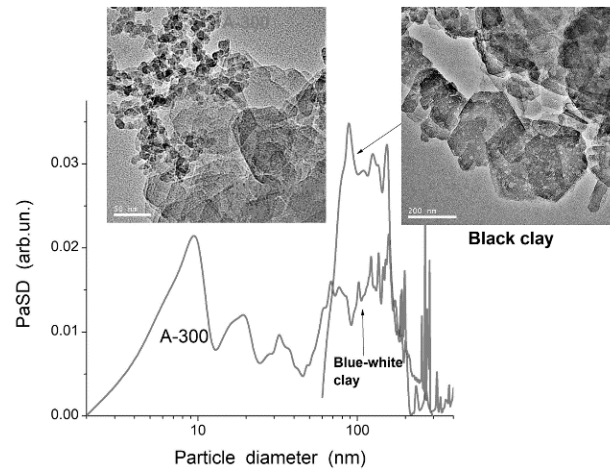

Fig. 8. Representative particle size distributions (PaSD) for black clay alone and blue-white clay/A−300 calculated using TEM images treated with ImageJ/granulometry (see details in [29])
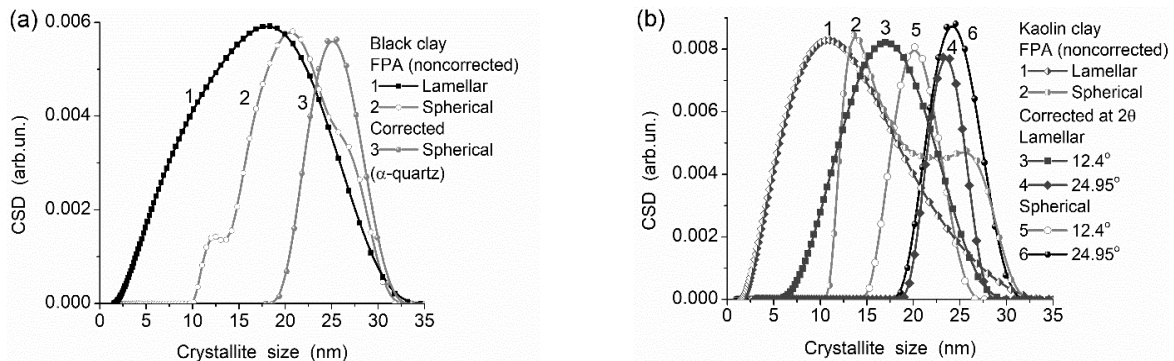

Fig. 9. CSD for (*a*) black clay and (*b*) kaolin clay calculated with FPA (without correction) and main peaks (with correction using models of spherical and lamellar crystallites)

Comparison of the CSD (Fig. 9) and PaSD (Fig. 8) shows that relatively large lamellar clay particles have much smaller thickness because the CSD function for the lamellar model corresponds to the lamellar thickness.

CONCLUSION

In this work, a method based on X-ray diffraction data and TEM images was developed to analyze the particulate and crystalline morphology of various metal and metalloid oxides comparing the CSD (XRD) and PaSD (TEM) functions. Two versions of the XRD treatment method were used: (i) full profile analysis of whole XRD patterns with a self-consistent regularization procedure using models of spherical and lamellar crystallites; and (ii) analysis of main XRD lines with consideration of corrections on the instrumental line profile caused by the equipment effects. These approaches were used for the characterization of the particulate (TEM) and crystalline (XRD) morphology of various materials: complex fumed oxides with silica/alumina, silica/titania and alumina/silica/titania; nanocomposites CeO_2–ZrO_2/SiO_2 (10 : 10 : 80 wt. %) and TiO_2–ZrO_2/SiO_2 (10 : 10 : 80 wt. %) synthesized using a liquid-phase method and fumed silica A–300 as a substrate; and natural clays of complex composition. Obtained results show that the developed XRD approaches could be effectively used in parallel with TEM images treatment for detailed descriptions of the particulate and crystalline morphology of various complex materials. The regularization procedures (including SCR) could be used to treat various indirect (with respect to the particulate and crystalline morphology) experimental data, such as XRD, SAXS, adsorption, *etc.*, for detailed characterization of complex materials and hybrid composites including several crystalline and amorphous phases, porous or highly disperse particles. The most appropriate results could be obtained using the approaches with the XRD line corrections on the instrumental line profile and TEM images treatment.

Морфологія частинок наноструктурованих матеріалів

В.М. Гунько, О.І. Оранська, В.В. Паєнтко, І.Я. Сулим

Інститут хімії поверхні ім. О.О. Чуйка Національної академії наук України
вул. Генерала Наумова, 17, Київ, 03164, Україна, vlad_gunko@ukr.net

Метою цього дослідження була розробка методу аналізу морфології частинок та кристалітів різних високодисперсних, складних оксидів металів та неметалів, що включають як кристалічні, так і аморфні фази, з використанням даних рентгенофазового аналізу (РФА) для розрахунків розподілу кристалітів за розміром (РКР) у порівнянні з розподілами частинок та кристалітів за розміром, що розраховані на основі зображень трансмісійної електронної спектроскопії високої роздільної здатності (ТЕМ), аналізованих з використанням специфічного програмного забезпечення. Було використано дві версії методу розрахунків на основі даних РФА: (і) повнопрофільний аналіз всієї рентгенограми з використанням самоузгодженої регуляризації та моделей сферичних та шаруватих частинок, що дозволяла визначити внески кристалітів різного типу, (іі) аналіз тільки основних РФА ліній з урахуванням поправок на профіль смуг приладу та базову лінію з використанням регуляризації і моделей сферичних або шаруватих кристалітів. Наближення на основі РФА та ТЕМ даних було тестовано для розрахунків морфології частинок та кристалітів різних систем: складних (бі- та трифазних) пірогенних оксидів SiO_2/Al_2O_3, SiO_2/TiO_2, Al_2O_3/SiO_2/TiO_2, що включали кристалічні фази Al_2O_3 та TiO_2 та аморфну фазу SiO_2; нанокомпозитів CeO_2–ZrO_2/SiO_2 (10 : 10 : 80 мас. %) та TiO_2–ZrO_2/SiO_2 (10 : 10 : 80 мас. %), що мали кристалічні та аморфні фази та які було синтезовано рідкофазним методом з використанням пірогенного кремнезему А-300 як носія; та природних глин зі складною будовою, що включали кілька кристалічних фаз. Отримані результати свідчать про те, що розроблений підхід на основі аналізу РФА даних для розрахунків РКР може бути ефективно використано паралельно з аналізом ТЕМ зображень з

V.M. Gun'ko, O.I. Oranska, V.V. Paientko, I.Ya. Sulym

використанням специфічного програмного забезпечення для детального опису морфології частинок та кристалітів різних дисперсних матеріалів.

Ключові слова: *складні пірогенні оксиди, нашаровані оксиди, глини, морфологія частинок, розподіл кристалітів за розміром*

Морфология частиц наноструктурованных материалов

В.М. Гунько, Е.И. Оранская, В.В. Паентко, И.Я. Сулим

Институт химии поверхности им. А.А. Чуйко Национальной академии наук Украины
ул. Генерала Наумова, 17, Киев, 03164, Украина, vlad_gunko@ukr.net

Целью данного исследования была разработка метода анализа морфологии частиц и кристаллитов различных высокодисперсных, сложных оксидов металлов и неметаллов с использованием данных рентгенофазового анализа (РФА) для расчетов распределений кристаллитов по размерам (РКР) в сравнении с распределениями частиц и кристаллитов по размерам, которые рассчитаны на основе изображений трансмиссионной электронной микроскопии высокого разрешения (ТЭМ). Было использовано две версии метода расчетов на основе данных РФА: (i) полнопрофильный анализ всей рентгенограммы с использованием самосогласованной регуляризации и моделей сферических и слоистых частиц, которая позволяла оценить вклады кристаллитов разных типов, (ii) анализ только основных РФА линий с учетом поправок на приборные эффекты и базовую линию с использованием метода регуляризации и моделей сферических и слоистых кристаллитов. Приближение, основанное на данных РФА и ТЭМ методов, было протестировано в рамках расчетов морфологии частиц и кристаллитов разных систем: сложных (двухфазных и трехфазных) пирогенных оксидов SiO_2/Al_2O_3, SiO_2/TiO_2, $Al_2O_3/SiO_2/TiO_2$, которые включали кристаллические фазы Al_2O_3 и TiO_2 и аморфную фазу SiO_2; нанокомпозитов $CeO_2–ZrO_2/SiO_2$ (10 : 10 : 80 масс. %) и $TiO_2–ZrO_2/SiO_2$ (10 : 10 : 80 мас. %), которые включали кристаллические и аморфные фазы и были синтезированы жидкофазным методом с использованием пирогенного кремнезема А-300 в качестве носителя; и природных глин со сложной структурой, которые включали несколько кристаллических фаз. Полученные результаты свидетельствуют о том, что разработанный подход на основе РФА данных для расчетов РКР может быть эффективно использован параллельно с численным анализом ТЭМ изображений с использованием специфического программного обеспечения для детального описания морфологии частиц и кристаллитов различных дисперсных материалов.

Ключевые слова: *сложные пирогенные оксиды, наслоенные оксиды, глины, морфология частиц, распределение кристаллитов по размерам*

REFERENCES

1. *Ullmann's Encyclopedia of Industrial Chemistry*. (Weinheim:Wiley-VCH, 2008).
2. Kulkarni P., Baron P.A., Willeke K. *Aerosol Measurement: Principles, Techniques, and Applications.* Third Edition. (New York: John Wiley & Sons, 2011).
3. Büchel K.H., Moretto H.-H., Woditsch P. *Industrial inorganic chemistry*. (Weinheim: Wiley-VCH Verlag GmbH, 2000).
4. Piemonte V., De Falco M., Basile A. *Sustainable Development in Chemical Engineering – Innovative Technologies. First Edition*. (UK, Chichester: John Wiley & Sons, 2013).
5. Camenzind A., Caseri W.R., Pratsinis S.E. Flame-made nanoparticles for nanocomposites. *Nano Today*. 2010. **5**(1): 48.
6. Fultz B., Howe J. *Transmission Electron Microscopy and Diffractometry of Materials.* (Berlin: Springer, 2007).
7. Stokes D.J. *Principles and Practice of Variable Pressure Environmental Scanning Electron Microscopy (VP-ESEM)* (Chichester: John Wiley & Sons, 2008).
8. Sakurai S. SAXS evaluation of size distribution for nanoparticles. Chapter 5 (http://dx.doi.org/10.5772/105981), In A.E. Ares (editor). *X-ray Scattering*. (Croatia: InTech, 2017). P. 107.

9. Brumberger H. *Small Angle X-ray Scattering*. (New York, Syracuse: Gordon & Breach, 1965).
10. Sztucki M., Narayanan T. Development of an ultra-small-angle X-ray scattering instrument for probing the microstructure and the dynamics of soft matter. *J. Appl. Crystallogr.* 2007. **40**: s459.
11. Buschow K.H.J. *Encyclopedia of Materials: Science and Technology*. (Amsterdam: Elsevier, 2001).
12. Cullity B.D., Stock S.R. *Elements of X-Ray Diffraction*. Third Edition. (New York: Prentice-Hall Inc., 2001).
13. David W.I.F., Shankland K., McCusker L.B., Baerlocher Ch. *Structure Determination form Powder Diffraction Data*. (London: Oxford Science, 2002).
14. Hunter R.J. *Introduction to Modern Colloid Science.* (London: Oxford University Press, 1993).
15. Gun'ko V.M., Zarko V.I., Leboda R., Chibowski E. Aqueous suspensions of fumed oxides: particle size distribution and zeta potential. *Adv. Colloid Interface Sci.* 2001. **91**: 1.
16. Gun'ko V.M. Various methods to describe the morphological and textural characteristics of various materials. *Him. Fiz. Tehnol. Poverhni.* 2018. **9**(1): 317.
17. Gun'ko V.M. Composite materials: textural characteristics. *Appl. Surf. Sci.* 2014. **307**: 444.
18. Guinier A. *X-Ray Diffraction.* (San Francisco: WH Freeman, 1963).
19. de Avillez R.R., Abrantes F.G., Letichevsky S. On the intrinsic limits of the convolution method to obtain the crystallite size distribution from nanopowders diffraction. *Mater. Res.* 2018. **21**(3): e20170980.
20. Popović S., Skoko Ž. X-ray diffraction broadening analysis. *Maced. J. Chem. Chem. Eng.* 2015. **34**(1): 39.
21. Provencher S.W. A constrained regularization method for inverting data represented by linear algebraic or integral equations. *Comput. Phys. Commun.* 1982. **27**(3): 213.
22. Image J. 2020. https://imagej.nih.gov/ij/, https://imagej.nih.gov/ij/plugins/granulometry.html.
23. Gun'ko V.M., Zarko V.I., Goncharuk O.V., Matkovsky A.K., Remez O.S., Skubiszewska-Zięba J., Wojcik G., Walusiak B., Blitz J.P. Nature and morphology of fumed oxides and features of interfacial phenomena. *Appl. Surf. Sci.* 2016. **366**: 410.
24. Gun'ko V.M., Turov V.V., Zarko V.I., Goncharuk O.V., Pahklov E.M., Skubiszewska-Zięba J., Blitz J.P. Interfacial phenomena at a surface of individual and complex fumed nanooxides. *Adv. Colloid Interface Sci.* 2016. **235**: 108.
25. Gun'ko V.M., Turov V.V. *Nuclear Magnetic Resonance Studies of Interfacial Phenomena*. (Boca Raton: CRC Press, 2013).
26. Sulym I., Sternik D., Oleksenko L., Lutsenko L., Borysenko M., Derylo-Marczewska A. Highly dispersed silica-supported ceria–zirconia nanocomposites: Preparation and characterization. *Surf. Interfaces*. 2016. **5**: 8.
27. Sulym I., Goncharuk O., Skwarek E., Sternik D., Borysenko M.V., Derylo-Marczewska A., Janusz W., Gun'ko V.M. Silica-supported ceria–zirconia and titania–zirconia nanocomposites: Structural characteristics and electrosurface properties. *Colloids Surf. A*. 2015. **482**: 631.
28. Sulym I., Goncharuk O., Sternik D., Skwarek E., Derylo-Marczewska A., Janusz W., Gun'ko V.M. Silica-supported titania–zirconia nanocomposites: Structural and morphological characteristics in different media. *Nanoscale Res. Lett.* 2016. **11**(111): 1.
29. Protsak I., Paientko V.V., Oranska O.I., Gornikov Yu.I., Prokhnenko P.A., Alekseev S.A., Babenko L.M., Liedienov N.A., Pashchenko A.V., Levchenko G.G., Gun'ko V.M. Interfacial phenomena in natural nanostructured materials based on kaolinite and calcite in blends with nanosilica and neem leaf powder. *Colloids Surf. A*. 2020. **586**: 124238.
30. *JCPDS Database*, International Center for Diffraction Data, PA, 2001.
31. Gun'ko V.M., Turov V.V., Goncharuk O.V., Pakhlov E.M., Matkovsky O.K. Interfacial phenomena at a surface of individual and complex fumed nanooxides. *Surface*. 2019. **11**(26): 3.
32. Gun'ko V.M. Nano/meso/macroporous materials characterization affected by experimental conditions and features of the used methods. *Him. Fiz. Tehnol. Poverhni.* 2020. **11**(1): 5.